



CHORUS

This is the accepted manuscript made available via CHORUS. The article has been published as:

Electronic structure and optical conductivities of 20 MAX-phase compounds

Yuxiang Mo, Paul Rulis, and W. Y. Ching

Phys. Rev. B **86**, 165122 — Published 16 October 2012

DOI: [10.1103/PhysRevB.86.165122](https://doi.org/10.1103/PhysRevB.86.165122)

Electronic Structure and Optical Conductivities of 20 MAX-Phase Compounds

Yuxiang Mo, Paul Rulis, and W.Y. Ching

Department of Physics, University of Missouri-Kansas City, Kansas City, Missouri 64110, USA

Abstract

The electronic structure and optical conductivities of 20 so-called MAX phases Ti_3AC_2 ($A = Al, Si, Ge$), Ti_2AC ($A = Al, Ga, In, Si, Ge, Sn, P, As, S$), Ti_2AlN , M_2AlC ($M = V, Nb, Cr$), and $Ta_{n+1}AlC_n$ ($n = 1$ to 4) are studied using the first-principles orthogonalized linear combination of atomic orbitals (OLCAO) method. The calculated results include total and partial density of states, effective charge on each atom and quantitative bond order values. Also calculated are directionally resolved interband optical conductivities. By analyzing such results regarding these phases (that have different atomic compositions and layered structures) several important features on structural stability and electrical conductivities are identified and compared with experimental data. We confirm the trend of increasing $N(E_f)$ (total density of states at the Fermi-level E_f) as the number of valence electrons of the composing elements increases. The local feature of total density of states (TDOS) near E_f is used to predict structural stability. The calculated effective charge on each atom shows that the M (transition-metal) atoms always lose charge to the X (C or N) atoms whereas the A-group atoms mostly gain charge but some lose charge. Bond order values are obtained and critically analyzed for all types of interatomic bonds in all the 20 MAX phases.

PACS numbers: 71.20.-b, 71.20.Be, 72.15.Eb, 78.66.Sq

1. INTRODUCTION

Originally studied in the 1960s,¹⁻⁷ the layered ternary transition-metal carbides and nitrides (also known as MAX phases) have the formula $M_{n+1}AX_n$, in which “M” represents a transition-metal (Ti, V, Cr, Nb, Ta, etc.), while “A” means a group III, IV, V, or VI element (Al, Ga, In, Si, Ge, Sn, P, As, S, etc.) from the periodic table, and “X” is either carbon or nitrogen. MAX phases have some outstanding properties and behave like both a metal and a ceramic. Like metals, they have good thermal and electrical conductivity, thermal shock resistance, machinability, and damage tolerance.⁸ Like ceramics, they are light-weight, stiff, refractory, and oxidation resistant.⁸ It is not surprising that there has been an upsurge of research activities on MAX phases by both experimentalists and theorists in recent years.⁸⁻¹² In terms of any one single property there is always a better material, but with the combination of the above mentioned features MAX-phase compounds have become highly regarded candidates for various technological and engineering applications. Current and future applications include high-temperature structural materials, porous exhaust gas filters for automobiles, heat exchangers, heating elements, wear and corrosion protective surface coatings, electrodes, resistors, capacitors, nuclear applications,^{13, 14} bio-compatible materials, rotating electrical contacts, cutting tools, nozzles, tools for die pressing, and impact-resistant materials such as projectile proof armor.⁸⁻¹⁰

Unlike other classes of materials, the MAX family includes more than 70 compounds,⁹ a number that is still increasing. A careful and systematic study of their properties and trends is thus of vital importance for deep understanding of the known phases and the quests to

discover new ones. In spite of the fact that some existing publications^{11, 15-19} have already addressed the electronic structure of MAX phases, a comprehensive and systematic study of a large number of MAX phases using a single computational method would be particularly helpful for the rational analysis of overall trends in their properties. One example property in MAX-phase compounds that has been recognized by many researchers is the nature of bonding, and another example that has not been as widely recognized but which is an important property nonetheless is the optical conductivity. They have been investigated by only a few groups and a comprehensive and quantitative analysis is presently lacking.

In this paper we report the electronic structure, bonding information, and optical conductivities of 20 MAX-phase compounds: Ti_3AC_2 ($A = Al, Si, Ge$), Ti_2AC ($A = Al, Ga, In, Si, Ge, Sn, P, As, S$), Ti_2AlN , M_2AlC ($M = V, Nb, Cr$) and $Ta_{n+1}AlC_n$ ($n = 1$ to 4). Most of them are titanium-containing phases, since they are the most common in MAX phases. The first twelve of the above-mentioned phases vary only by the A element, for the purpose of studying the changes caused by A element variations, both among the three (3 1 2) phases, and the nine (2 1 1) phases. In addition to carbides, one example of nitride, Ti_2AlN has also been included here. This is followed by three other (2 1 1) phases, $(V, Nb, Cr)_2AlC$, varying by the M element, again for the trend observation. The Ta-Al-C phases are chosen to study the effect of the number of MX layers. In Sec. 2, the crystal structures of these layered compounds are briefly discussed. The method of calculation is described in Sec. 3. The main section, Sec. 4, details the results and discusses them. In the last section, Sec. 5, we present our summary of the present work.

2. CRYSTAL STRUCTURES

MAX-phase crystals have a hexagonal symmetry in space group $P6_3/mmc$ (#194) with Wyckoff positions: M (4*f*), A (2*d*), and X (2*a*) for (2 1 1); M1 (4*f*), M2 (2*a*), A (2*b*), and X (4*f*) for (3 1 2); M1 (4*e*), M2 (4*f*), A (2*c*), X1 (4*f*) and X2 (2*a*) for (4 1 3); M1 (4*f*), M2 (4*f*), M3 (2*a*), A (2*c*), X1 (4*e*) and X2 (4*f*) for (5 1 4) phases. Listed in Table 1 are the lattice constants and internal parameters (z (M) and z (C)) used in present calculation. The crystal structure consists of $M_{n+1}X_n$ slabs and intercalation of planar packed A-group atoms.⁹ Fig. 1 shows the structures of the Ta-Al-C family (Ta_2AlC (2 1 1), α - Ta_3AlC_2 (3 1 2), α - Ta_4AlC_3 (4 1 3), and Ta_5AlC_4 (5 1 4) phases). The simplest structure is Ta_2AlC in Fig. 1 where Ta, C, and Al atoms form hexagonal near close-packed layers. The unit cell contains a total of 8 atoms with Ta, Al, and C occupying unique positions. In the (3 1 2) phase, there are 12 atoms in the unit cell (4 Ta1, 2 Ta2, 2 Al, and 4 C) with two crystallographically nonequivalent Ta sites (Ta1 and Ta2) and unique sites for Al and C. There are 16 atoms in the unit cell of α - Ta_4AlC_3 and it has 2 types of Ta and 2 types of C (4 Ta1, 4 Ta2, 2 Al, 4 C1, and 2 C2). Finally, Ta_5AlC_4 has 20 atoms in the unit cell with 3 types of Ta and 2 types of C (4 Ta1, 4 Ta2, 2 Ta3, 2 Al, 4 C1, and 4 C2). In MAX-phase compounds, increasing the number of stacking layers of M and X atoms complicates the interatomic bonding, and this will be discussed in Section 4.2. Most of the crystals in the present study are (2 1 1) and (3 1 2) phases.

3. METHOD OF CALCULATION

The electronic structure and optical conductivities of the MAX phases were calculated using the first-principles orthogonalized linear combination of atomic orbitals (OLCAO) method²⁰ which is based on the local density approximation (LDA) of density functional theory.^{21, 22} This

method has been demonstrated to be highly accurate and efficient when dealing with materials with complex structures for both crystalline²³⁻²⁹ and non-crystalline systems³⁰⁻³⁴. In the OLCAO method, the solid state wave functions are expanded in atomic orbitals which consist of Gaussians type orbitals (GTOs) and spherical harmonics appropriate for the angular momentum quantum number. Three types of basis set were used. The full basis (FB), which consists of the core orbitals, occupied valence orbitals, and the next empty shell of unoccupied orbitals for each atom, is used for the determination of the self-consistent potential and subsequent calculations of band structure and density of states (DOS). Taking Ti_3AlC_2 as an example, the FB has atomic orbitals of Ti-($1s, 2s, 2p, 3s, 3p, 3d, 4s, 4p$), Al-($1s, 2s, 2p, 3s, 3p, 3d$) and C-($1s, 2s, 2p, 3s, 3p$). With 12 atoms in the unit cell, the dimension of the secular equation for Ti_3AlC_2 after core orthogonalization is only 166×166 . In the calculation of optical conductivities, an extended basis (EB) set was used, which include one additional shell of empty orbitals to improve the accuracy of the higher states in the conduction band. On the other hand, for the effective charge and bond order calculations using Mulliken analysis,³⁵ a minimal basis (MB) was used which provides a more localized basis for such analysis. The crystal potential achieved self-consistency in about 35 iterations when the total energy converged to less than 0.0001 a.u. difference. A large k -point sampling of at least 408 k points in the irreducible portion of the Brillouin zone were used. Additional tests with more k points showed no discernible differences. The versatility of using different basis sizes for different purposes is instrumental in enabling the OLCAO method to have high efficiency and accuracy for calculations of a variety of properties.

In addition to the usual band structure and DOS calculations, one of the most useful features of the OLCAO method is the quantitative evaluation of the effective charge Q^* on each atom and the bond order (BO) values for each pair of atoms in the crystal without any assumption on atomic size or radius. They are evaluated according to:

$$Q_{\alpha}^* = \sum_i \sum_{n,occ} \sum_{j,\beta} C_{i\alpha}^{n*} C_{j\beta}^n \langle b_{i\alpha}(\vec{k}, \vec{r}) | b_{j\beta}(\vec{k}, \vec{r}) \rangle \quad (1),$$

$$\rho_{\alpha\beta} = \sum_{n,occ} \sum_{i,j} C_{i\alpha}^{n*} C_{j\beta}^n \langle b_{i\alpha}(\vec{k}, \vec{r}) | b_{j\beta}(\vec{k}, \vec{r}) \rangle \quad (2).$$

In Eq. (2), the $\rho_{\alpha\beta}$ denotes the bond order for the atom pair (α, β); n is the band index; i and j are the orbital quantum numbers and the C 's are the eigenvector coefficients of the Bloch function $b(\vec{k}, \vec{r})$.

For the calculation of interband optical conductivities, the imaginary component of the dielectric function was evaluated first, using:

$$\varepsilon_2(\omega) = \left(\frac{e^2}{\pi m E \omega} \right) \times \int d\vec{k} \sum_{n,l} \left| \langle \psi_n(\vec{k}, \vec{r}) | \vec{P} | \psi_l(\vec{k}, \vec{r}) \rangle \right|^2 f_l(\vec{k}) \times [1 - f_n(\vec{k})] \delta[E_n(\vec{k}) - E_l(\vec{k}) - E] \quad (3),$$

where $E = \hbar\omega$ is the photon energy; l stands for an occupied state and n an unoccupied state;

$\psi_n(\vec{k}, \vec{r})$ is the Bloch wave function for the n^{th} band with energy $E_n(\vec{k})$ at Brillouin zone point k ;

$f(\vec{k})$ is the Fermi distribution function. The momentum matrix element (MME)

$\langle \psi_n(\vec{k}, \vec{r}) | \vec{P} | \psi_l(\vec{k}, \vec{r}) \rangle$ was explicitly calculated from the *ab initio* wave functions. The real part

of the optical conductivity $\sigma_1(\hbar\omega)$ is obtained from $\sigma_1(\hbar\omega) = \frac{\varepsilon_2\omega}{4\pi}$. The information on the

anisotropy in the optical conductivities can be obtained by resolving the square of the MME into specific Cartesian components.

4. RESULTS AND DISCUSSION

4.1 Total and Partial Density of States

Fig. 2 shows the calculated total and partial (atom-resolved) DOS of all the 20 MAX-phase compounds, for the benefit of handy comparison by readers with results from alternative sources. The band structures were also obtained but are not presented here. For metallic phases, the DOS at the Fermi-level is a key quantity. Table 2 lists the calculated $N(E_f)$ values (and their atom-resolved components) in comparison with quoted values from the literature. Those values with an asterisk come from experiments. We were unable to find any previously reported results for Ta_5AlC_4 . As can be seen, results from different research groups can vary significantly, indicating the ambiguity for this most fundamental quantity. Due to the phonon-electron coupling, the empirical $N(E_f)$ results from specific heat measurements differ a lot from theoretical values, especially in the case of Cr_2AlC ,³⁶ with a $\sim 100\%$ deviation. This underscores the importance of having a consistent set of results calculated using a single method for trend analysis.

In Fig. 3, we plot the $N(E_f)$ for 14 of these phases in columns of 3, 4, 5, and 6 valence electrons in order to show the trends in accordance with the valence electron fillings of each type of the composing elements. They are consistent with Hug's observation.³⁷ For the nine (2 1 1) phases shown in Fig. 3(a), the $N(E_f)$ increases with the filling of p electrons of the A elements. The $N(E_f)$ has a much larger difference between Ti_2InC and Ti_2SnC than between

Ti_2GaC and Ti_2GeC . This can be explained by the fact that the single $5p$ valence electron difference between In and Sn has higher energy than the $4p$ electron difference between Ga and Ge, thus contributing more states to the Fermi-level. In the same sense, the $N(E_f)$ difference between Ti_2GaC and Ti_2GeC is also larger than that between Ti_2AlC and Ti_2SiC , however with a much smaller difference. In Fig. 3(b), the same trend of larger $N(E_f)$ with a larger number of valence electrons also applies to the two (3 1 2) phases Ti_3AlC_2 and Ti_3SiC_2 . This trend can also be observed in the variations of the M element (Ti_2AlC , V_2AlC , Cr_2AlC) and the X element (Ti_2AlC , Ti_2AlN). Thus, our data supports the notion that the increase of valence electrons of A, M, and X elements tends to coincide with an increase of $N(E_f)$. An exception is Ti_2SC , which has a much smaller $N(E_f)$ compared with that of Ti_2PC despite the fact that S has one more valence electron than P does. This anomaly was also observed in Hug's³⁷ calculation, in which the orbital-resolved DOS was analyzed. It was found that the substitution of P with S does not substantially change the shape of the Ti- $3d$ curve, but rather it shifts the Fermi-level from the peak to the valley in the Ti- $3d$ DOS, resulting in a large decrease in $N(E_f)$. Such a shift was believed to be caused by the strengthening M-A bond which was based on the observation that the S- $3p$ and Ti- $3d$ states have significant energy overlaps near -3.5 eV. The Ti-S bond was even predicted to be stronger than the Ti-C bond. However, in the present work, the calculated bond order results (detailed in Sec. 4.2) suggest otherwise. The Ti-S bond order (0.165) is actually lower than the Ti-P bond order (0.199), along with a larger bond length (Ti-S 2.511 Å > Ti-P 2.505 Å). This reminds us that the correlation between electrons favoring the same energy states and the participation of such electrons in bonding is not always reliable.

Theoretically explained³⁸, experimentally verified^{39, 40}, and often adopted^{37, 41, 42}, the local features of the TDOS curve around the Fermi-level can be a reasonable indicator of the intrinsic stability of a crystal. A local minimum at E_f implies higher structural stability because it signifies a barrier for electrons below the Fermi-level ($E < 0$ eV) to move into unoccupied empty states ($E > 0$ eV); whereas a local maximum at E_f is usually a sign of structural instability. This qualitative criterion could work well, only on those with prominent dips and peaks in the DOS at the Fermi-level. We have selected such compounds the DOS of which are plotted in Fig. 4. Ti_2InC , Ti_2SC , and Cr_2AlC have their E_f located at a local minimum in the TDOS, suggesting a higher level of stability. This is indirectly supported by the ease with which these phases can be synthesized.⁴³⁻⁴⁵ In fact, Ti_2InC was one of the earliest MAX phases successfully fabricated.² On the other hand, Ti_2PC , Ti_2AsC , and Ta_5AlC_4 show a peak in the TDOS at the Fermi-level. To the authors' knowledge, pure Ti_2PC or Ti_2AsC has never been synthesized, which agrees with our observation. From the plot, Ti_2AsC has the same basic shape of TDOS curve as that of Ti_2PC , which is not surprising since P and As are isoelectronic. However, the Fermi-level in Ti_2AsC lies in a shallow minimum within a narrow plateau between -0.5 eV and 0.5 eV. This gives Ti_2AsC slightly higher phase stability. For Ta_5AlC_4 , the Fermi-level is located at a very sharp peak and this is consistent with the fact that successful synthesis of Ta_5AlC_4 has never been reported.⁴⁶ Our predictions of the contrasting stability of Ti_2SC and Ti_2PC crystals are consistent with the calculations by Du et al.¹⁶ and Hug et al.³⁷. Nevertheless, for those other phases, their less salient DOS topography at the Fermi-level could be outweighed by other factors in determining the phase stability, especially further in predicting whether a phase can exist or not. An

example would be Ti_2SiC , which has not been reported to exist as a single phase, presumably because of the competition from other phases in the Ti-Si-C phase diagram¹⁰.

4.2 Effective Charge and Bond Order

The effective charge Q^* on each atom and the bond order values for each pair of atoms in the 20 MAX-phase compounds were calculated according to Eqs. (1) and (2). The charge deviations from the neutral atom (charge gains or losses) are listed in Table 2 and plotted in Fig. 5. The amount of charge transfer can characterize the degree of ionicity in a certain MAX-phase compound. It can be seen that the transition-metal atoms always lose charge and C or N always gain charge (more negative). Whereas for A atoms, most of them also gain charge but some lose a tiny amount. An exception is in Cr_2AlC where Al loses almost 0.33 electron with a concomitant large gain of charge by C (0.52 electron) and the smallest charge loss from a transition-metal element (0.09 electron). This is in sharp contrast with Nb_2AlC where Nb loses 0.51 electron and C and Al gain 0.74 and 0.28 electron respectively. Thus, from a charge-transfer point of view, Cr_2AlC is clearly an outlier among the 20 MAX-phase compounds. A trend in the Ta-Al-C series is also observed in the figure. As the stoichiometric ratio of Ta to C decreases there are more C atoms per Ta such that in the limit of large n the degree of electron transfer approaches that of TaC. The charge transfer in MAX-phase compounds has also been studied by others⁴⁷. The calculation of effective charge and charge transfer in any crystal depends on the methods employed and the definition used. Unlike the plane-wave based methods where the atomic radius have to be assumed when the charges are calculated, the OLCAO method⁴⁸ does not have such a somewhat arbitrary assumption and the results are far

more reliable. In compounds with simple structures and bonding, the difference may be small. However, the MAX-phase compounds have complex layered structure and different types of bonding, it is only natural that their results on charge transfer differ from ours.

In MAX-phase type compounds the unique structure and different types of bonding make quantitative bond order (BO) values based on rigorous quantum mechanical calculations particularly valuable. Listed in Table 3 are the calculated BO values which have been categorized for each bonding type in the 20 MAX-phase compounds. In the heading of Table 3, “M-X” denotes the bonding between the transition-metal M and C (or N). “M-A” represents the bonding between M and A-group atoms. “M-M” indicates the bonding between the transition-metal atoms. If the two M atoms belong to the same layer, the bonding is labeled “Intra-layer”. If they belong to two different layers, it is designated as “Inter-layer”. If the two layers are separated by an X (A) atom layer, it is labeled as a “Cross X (A)” type of bonding. Finally, “A-A” labels the bonding between A-group atoms. For (3 1 2), (4 1 3), and (5 1 4) phases, the M-X and M-M bonds have diverse types due to the presence of crystallographically non-equivalent M and X sites discussed in Sec. 2. This is illustrated in Fig. 6 for Ta_2AlC , $\alpha-Ta_3AlC_2$, $\alpha-Ta_4AlC_3$, and Ta_5AlC_4 . In Ta_2AlC , the upper two Ta layers are equivalent, thus the M-X and M-M bonds have no complications. An additional Ta layer (below the Al layer) is displayed, to help visualize the “Cross A” M-M bonding, which exists only in Ti_2PC and Ti_2SC . For $\alpha-Ta_3AlC_2$, there are three Ta layers and two C layers, which are broken down to two Ta sites (Ta1 and Ta2) and one C site. The M-X bonding therefore includes M2-C and C-M1 which are distinguished in Table 3. The Intra-layer M-M bonding has M1-M1 and M2-M2 types which are abbreviated as “M1” and “M2”

respectively in Table 3. The Cross X M-M bonding has only one type: M1-M2. Similarly for α - Ta_4AlC_3 and Ta_5AlC_4 , M-X and M-M bonds are also subdivided into multiple categories in Table 3.

Based on the BO values listed in Table 3, we can summarize several important observations:

(1) The highest BO in these MAX-phase compounds are for the M-X bonds, ranging from 0.150 to 0.230, followed by the M-A bonds with BO values from 0.110 to 0.199. The M-M and A-A bonds have relatively smaller BO values of 0.020 to 0.096 for M-M bonds and 0.0 to 0.074 for A-A bonds.

(2) The M-M bonding includes not only those bonds within a certain M layer (“Intra-layer”), but also the bonding between two M layers (“Inter-layer”) separated by either an X (“Cross X”) or an A (“Cross A”) layer. For the Cross X inter-layer M-M bonding, each M atom forms 3 bonds with the 3 nearest M atoms in the next M layer. According to the present calculation, X-X atom pairs in the 20 MAX-phase compounds do not form bonds. This proves that in these compounds the X layer has no intrinsic cohesion. Its structure is solely based on the structures of the two nearby M layers via the strong M-X bonds.

(3) It is important to realize that both the magnitudes of the BO and the number of bonds can contribute to the cohesion of a compound. Within each M layer, each M atom forms 6 bonds with 6 adjacent M atoms. However, an M atom forms only 3 M-X (M-A) bonds with the 3 nearest X (A) atoms in the next layer. Besides, M-X (M-A) bonds also contribute to the in-layer cohesion because such bonds are not perpendicular to the layers. Thus even though the individual BO numbers for M-X and M-A bonds may seem much larger than those for intra-layer M-M and A-A bonds, the overall inter-layer M-X (M-A) bonding is not so much stronger,

especially the M-A. The weakness of the M-A bonding compared to the M-X bonding can also be attributed to their comparatively larger bond lengths. For the 20 MAX-phase compounds, the M-A bond lengths range from 2.50 to 3.02 Å, which are 20~40% larger than the M-X bond lengths, that range from 1.98 to 2.17 Å. This weak interaction between the M layer and the A layer is widely recognized to be the microscopic origin responsible for the machinability, thermal shock resistance, and damage (and defects) tolerance, properties that conventional brittle ceramics do not possess.⁸

(4) In Ti_3AlC_2 , Ti_3SiC_2 , and Ti_3GeC_2 , the “M2” bonds are weaker than the “M1” bonds. Therefore, when it comes to the intra-layer M-M bonding, the bonds near the A layer are stronger than those further away. Or in other words, the M layer that is next to the A layer is stronger than the one that is not. This is most evident in the case of the Ta-Al-C phases where the “M1” bond order values are almost 5 times as large as the values for the corresponding “M2” bonds. The comparatively strong intra-layer M-M bonding (BO ~ 0.095) near the A layer may be one of the reasons why Ta-Al-C phases have outstanding mechanical properties.⁴⁹

(5) There are several special cases worth mentioning. Amongst the 20 MAX-phase compounds studied, Ti_2PC and Ti_2SC have the unique “Cross A” type inter-layer M-M bonding. This is likely due to the relatively small atomic radius of P and S, which have brought the M layers at both sides closer to each other. The interatomic distances of such M-M pairs thus come to 3.394 Å in Ti_2PC and 3.382 Å in Ti_2SC , distances that are short enough for the bond formation. Unlike the Cross X inter-layer M-M bonding where each M atom forms 3 bonds with the 3 nearest M atoms in the next M layer, the Cross A inter-layer M-M bonding here is one-on-one. Besides, they are perpendicular to the layers, with no contribution to the in-layer cohesion. Ti_2PC , Ti_2AsC ,

and Ti_2SC have high M-X and M-A BO but very low intra-layer M-M BO and no A-A bonding. This could imply that they have a relatively larger mechanical anisotropy. On the other hand, Nb_2AlC has the lowest M-A and M-X BO and no inter-layer M-M bonding. This denotes the incorrectness of the previous comment⁴⁷ that the Nb-Al bond in Nb_2AlC was stronger than the Ti-Al bond in Ti_2AlC . Such a comment was based on the DOS overlap (already discussed in Sec. 4.1), visual observation of the charge density map (assumptions of atomic radius, Sec. 4.2), and the slightly larger bulk moduli (which is an unreliable indicator of bond strength) calculated for Nb_2AlC .

4.3 Optical Conductivities

We have calculated the interband optical conductivities σ_1 for the 20 MAX-phase compounds for frequency range between 0 and 10 eV using *ab initio* wave functions with an extended basis set and inclusion of the MME. Displayed in Fig. 7, they have been resolved into the planar and the axial (c-direction) components, or $\sigma_{1, planar}$ and $\sigma_{1, axial}$ for short. The number in each plot is the anisotropy ratio, which is the averaged ($\sigma_{1, planar}/\sigma_{1, axial}$) ratio over all the data points consisting the curves. From these plots, several interesting observations can be made.

(1) For the (Ti_2AlC , V_2AlC , Cr_2AlC) series with M elements in the 4th period of the periodic table, the axial curves have almost the same shape. The planar component has a slightly larger difference in shape, especially between V_2AlC and Cr_2AlC . For the (V_2AlC , Nb_2AlC , Ta_2AlC) series with M elements in the VA group of the periodic table, the main peak of the axial curve decays rapidly. But at energy levels near 0.0 eV, the axial component rises. The planar curve, on the contrary, is developing higher peaks. The anisotropy ratio in the series thus increases, from 1.47

to 1.81 and then 2.51. For the (Ti₂AlC, Ti₂SiC, Ti₂PC, Ti₂SC) series with A elements from the 3rd period of the periodic table, the anisotropy ratio increases in going from Ti₂AlC (1.23) to Ti₂SiC (1.41), but reduces when it gets to Ti₂PC (1.17), and then experiences only a slight decrease to 1.16 for Ti₂SC. Here the nonmetallic Phosphorous and Sulfur elements seem to play a significant role in this behavior. When the A element changes within the same isoelectronic group (Ti₃SiC₂, Ti₃GeC₂ and Ti₂PC, Ti₂AsC), both the axial and the planar curves remain almost the same.

(2) The optical conductivity may be expected to be a good gauge of photo-conductivity. Indeed, this was demonstrated in Nd₂CuO_{4-δ}⁵⁰ via simultaneous measurements of both the optical and photo-conductivity. Furthermore, the photo-conductivity could shed light on the electrical conductivity. In Fig.7, we notice that Nb₂AlC, Ta₂AlC, and Ta₅AlC₄ have the axial component of σ_1 increasing rapidly as $\hbar\omega$ goes to zero. Thus despite the fact that intraband optical conductivities are not included here, this might still be an indication for higher electrical conductivity in the axial direction compared to that in the planar direction. In fact, this has already been observed in Nb₂AlC.⁵¹

(3) It is conceivable that the anisotropy in optical conductivity in the low energy range (which is not to be confused with the averaged anisotropy ratio given in Fig. 7) could also imply that there are similar trends in the electrical conductivity. Besides the averaged anisotropy ratio, the degree of optical anisotropy in the low energy range of our calculation is also quite low for the majority of the 20 phases. This correlates well to the low anisotropy in the measured electrical conductivities.⁵²⁻⁵⁵ However, Nb₂AlC, Ta₂AlC and Ta₅AlC₄ have distinctly larger optical anisotropy as $\hbar\omega$ goes to zero. We thus expect the anisotropy of the electrical conductivities in Nb₂AlC,

Ta₂AlC and Ta₅AlC₄ to be higher. Indeed, experiments by T. H. Scabarozzi et al.⁵¹ showed that Nb₂AlC has a significantly larger anisotropy in its electrical conductivity than other MAX-phase compounds.

5. SUMMARY

In summary, we have performed a systematic first-principles calculation of the electronic structure and optical conductivities of 20 MAX-phase compounds. The results obtained by using a single computational method, the OLCAO method, enable us to observe the trends in various aspects of MAX-phase properties. The $N(E_f)$ was used to correlate the valence electron fillings and intrinsic structural stabilities. The calculated effective charge on each atom provides detailed information of the charge transfer in MAX-phase compounds and reveals the abnormal feature with Cr₂AlC. The bond order data provides detailed knowledge of the chemistry involved in MAX-phase compounds and an improved understanding of their intrinsic mechanical properties. The calculated anisotropic optical conductivities were used to predict the anisotropy of electrical conductivities. In spite of the detailed calculations for a large number of MAX-phase compounds that are presented in this paper, we must admit that consistent explanation of all the experimental data and trends is still not possible, especially those related to the bulk mechanical properties. This is due mainly to the fact that the MAX phase is a special class of layered ternary alloys with many diverse properties yet to be explored. From the experimental side, better sample characterization can narrow the uncertainty in the measured data. On the theoretical side, the ability to link the calculated results at the atomic

scale and at zero temperature to experimental data measured at the macro-scale and at finite temperature is an ongoing challenge.

Acknowledgements

This work was supported by the U.S. Department of Energy (DOE) – National Energy Technology Laboratory under Grant No. DE-FE0005865 and DE-FE0004007. This research used the resources of the National Energy Research Scientific Computing Center supported by the Office of Basic Science of DOE under Contract No. DE-AC03-76SF00098.

Tables:

Table 1. Crystal parameters of the 20 MAX-phase compounds

Crystal	a = b (Å)	c (Å)	z (M)	z (C)
Ti ₃ AlC ₂ ⁴	3.0753	18.578	0.128	0.564
Ti ₃ SiC ₂ ⁵⁶	3.0575	17.6235	0.1355	0.0722
Ti ₃ GeC ₂ ¹¹	3.077	17.76	0.1361	0.5737
Ti ₂ AlC ⁵⁷	3.04	13.6	0.086 ¹	
Ti ₂ GaC ³⁷	3.07	13.52	0.0848	
Ti ₂ InC ³⁷	3.13	14.06	0.0778	
Ti ₂ SiC ³⁷	3.052	12.873	0.0916	
Ti ₂ GeC ⁵⁸	3.079	12.93	0.0885 ³⁷	
Ti ₂ SnC ³⁷	3.163	13.679	0.0807	
Ti ₂ PC ³⁷	3.191	11.457	0.1019	
Ti ₂ AsC ³⁷	3.209	11.925	0.0943	
Ti ₂ SC ⁸	3.216	11.22	0.0993 ³⁷	
Ti ₂ AlN ⁴⁷	2.99	13.7	0.085	
V ₂ AlC ¹⁸	2.91	13.13	0.086	
Nb ₂ AlC ⁴⁷	3.119	13.77	0.0883	
Cr ₂ AlC ⁵⁹	2.86	12.8	0.086	
Ta ₂ AlC ⁴⁶	3.075	13.83	0.0833	
α-Ta ₃ AlC ₂ ⁴⁶	3.09	19.135	0.125	0.0625
α-Ta ₄ AlC ₃ ⁴⁶	3.112	24.111	0.15, 0.05	0.1
Ta ₅ AlC ₄ ⁴⁶	3.125	29.1	0.1667, 0.0833	0.125, 0.0417

Table 2. DOS (Total and Atom-Resolved) at E_f and charge transfer amounts

Crystal	$N(E_f)$	$N(E_f)$ M	$N(E_f)$ A	$N(E_f)$ X	$N(E_f)$ from literatures	ΔQ^* M	ΔQ^* A	ΔQ^* X
Ti_3AlC_2	3.83	2.97	0.67	0.19	$3.72^{11}, 3.34^{60}$	-0.430	-0.034	0.663
Ti_3SiC_2	4.45	3.32	0.89	0.24	$4.38^{11}, 4.76^{19}, 5^{*61}$	-0.481	0.105	0.669
Ti_3GeC_2	4.33	3.33	0.78	0.22	4.65^{11}	-0.562	0.357	0.667
Ti_2AlC	2.87	2.24	0.55	0.08	$2.67^{37}, 3.0^{18}, 4.32^{*36}$	-0.335	-0.022	0.694
Ti_2GaC	3.27	2.76	0.44	0.08	2.55^{37}	-0.496	0.294	0.698
Ti_2InC	2.54	2.14	0.34	0.06	2.39^{37}	-0.439	0.175	0.708
Ti_2SiC	3.15	2.36	0.69	0.10	3.17^{37}	-0.402	0.114	0.691
Ti_2GeC	3.59	2.76	0.73	0.10	3.83^{37}	-0.515	0.332	0.702
Ti_2SnC	3.53	2.80	0.63	0.10	3.71^{37}	-0.405	0.117	0.693
Ti_2PC	5.46	3.95	1.22	0.29	5.99^{37}	-0.459	0.217	0.701
Ti_2AsC	4.85	3.36	1.24	0.25	5.25^{37}	-0.518	0.342	0.700
Ti_2SC	1.98	1.72	0.20	0.06	1.55^{37}	-0.443	0.186	0.705
Ti_2AlN	3.92	3.06	0.72	0.14	$3.0^{17}, 5.38^{*36}$	-0.298	-0.083	0.679
V_2AlC	5.19	4.56	0.53	0.10	$6.0^{36}, 5.0^{18}, 7.98^{*36}$	-0.287	-0.077	0.658
Nb_2AlC	3.84	3.14	0.57	0.13	$3.78^{36}, 5.06^{*36}$	-0.511	0.280	0.742
Cr_2AlC	6.65	5.96	0.63	0.06	$6.0^{36}, 6.30^{18}, 12.92^{*36}$	-0.090	-0.334	0.517
Ta_2AlC	2.92	2.08	0.68	0.16	$\sim 3.4^{62}$	-0.357	-0.005	0.725
$\alpha-Ta_3AlC_2$	3.65	2.70	0.30	0.64	$\sim 2.2^{62}$	-0.447	-0.030	0.687
$\alpha-Ta_4AlC_3$	4.22	3.24	0.48	0.50	$6.76^{15}, \sim 5.6^{62}$	-0.500	-0.040	0.681
Ta_5AlC_4	12.40	8.52	0.80	3.08		-0.525	-0.042	0.670

Table 3. Calculated bond order values for the 20 MAX-phase compounds

Crystal	M-X				M-A	M-M					A-A
						Intra-layer		Inter-layer			
	Cross X		Cross A								
Ti ₂ AlC	0.212				0.159	0.069		0.050			0.063
Ti ₂ GaC	0.213				0.148	0.058		0.055			0.058
Ti ₂ InC	0.212				0.139	0.059		0.065			0.070
Ti ₂ SiC	0.214				0.173	0.052		0.042			0.031
Ti ₂ GeC	0.215				0.151	0.050		0.048			0.032
Ti ₂ SnC	0.214				0.152	0.054		0.056			0.040
Ti ₂ PC	0.216				0.199	0.029		0.041		0.053	
Ti ₂ AsC	0.216				0.171	0.029		0.052			
Ti ₂ SC	0.215				0.165	0.027		0.058		0.031	
Ti ₂ AlN	0.179				0.153	0.079		0.038			0.069
V ₂ AlC	0.205				0.152	0.070		0.037			0.072
Nb ₂ AlC	0.150				0.110	0.022					0.060
Cr ₂ AlC	0.197				0.153	0.049		0.022			0.074
Ta ₂ AlC	0.209				0.154	0.082		0.062			0.067
	M2-C	C-M1				M2		M1	M1-M2		
Ti ₃ AlC ₂	0.204	0.219			0.158	0.023		0.069	0.040		0.062
Ti ₃ SiC ₂	0.197	0.230			0.175	0.033		0.045	0.037		0.030
Ti ₃ GeC ₂	0.192	0.234			0.157	0.037		0.043	0.037		0.029
α-Ta ₃ AlC ₂	0.216	0.206			0.145	0.020		0.096	0.040		0.068
α-Ta ₄ AlC ₃	C2-Ta2	Ta2-C1		C1-Ta1	0.143	Ta2		Ta1	Ta2-Ta2	Ta2-Ta1	0.068
	0.216	0.218		0.206		0.021		0.095	0.025	0.044	
Ta ₅ AlC ₄	Ta3-C2	C2-Ta2	Ta2-C1	C1-Ta1	0.143	Ta3	Ta2	Ta1	Ta3-Ta2	Ta2-Ta1	0.066
	0.219	0.212	0.216	0.209		0.020	0.022	0.096	0.029	0.042	

References:

- 1 W. Jeitschko, H. Nowotny, and F. Benesovsky, Monatshefte fuer Chemie **94**, 672 (1963).
- 2 W. Jeitschko, H. Nowotny, and F. Benesovsky, Monatshefte fuer Chemie **94**, 1201 (1963).
- 3 D. I. Bardos and P. A. Beck, Transactions of the Metallurgical Society of AIME **236**, 64 (1966).
- 4 W. Jeitschko and H. Nowotny, Monatshefte fuer Chemie **98**, 329 (1967).
- 5 H. Wolfsgruber, H. Nowotny, and F. Benesovsky, Monatshefte fuer Chemie **98**, 2403 (1967).
- 6 H. Nowotny and F. Benesovsky, Planseeberichte fuer Pulvermetallurgie **16**, 204 (1968).
- 7 O. Beckmann, H. Boller, H. Nowotny, and F. Benesovsky, Monatshefte fuer Chemie **100**, 1465 (1969).
- 8 M. W. Barsoum, Progress in Solid State Chemistry **28**, 201 (2000).
- 9 J. Wang; and Y. Zhou, Annual Review of Materials Research **39**, 415 (2009).
- 10 P. Eklund, M. Beckers, U. Jansson, H. Hoegberg, and L. Hultman, Thin Solid Films **518**, 1851 (2010).
- 11 Y. Zhou, Z. Sun, X. Wang, and S. Chen, Journal of Physics: Condensed Matter **13**, 10001 (2001).
- 12 M. W. Barsoum and M. Radovic, Annual Review of Materials Research **41**, 195 (2011).
- 13 J. C. Nappé, P. Grosseau, F. Audubert, B. Guilhot, M. Beauvy, M. Benabdesselam, and I. Monnet, Journal of Nuclear Materials **385**, 304 (2009).
- 14 F. Meng, L. Chaffron, and Y. Zhou, Journal of Nuclear Materials **386-388**, 647 (2009).
- 15 Y. L. Du, Z. M. Sun, H. Hashimoto, and W. B. Tian, Solid State Communications **145**, 461 (2008).
- 16 Y. L. Du, Z. M. Sun, and H. Hashimoto, Physica B: Condensed Matter **405**, 720 (2010).
- 17 G. Hug and E. Fries, Physical Review B **65**, 113104 (2002).
- 18 Z. Sun, R. Ahuja, S. Li, and J. M. Schneider, Applied Physics Letters **83**, 899 (2003).
- 19 N. I. Medvedeva, D. L. Novikov, A. L. Ivanovsky, M. V. Kuznetsov, and A. J. Freeman, Physical Review B **58**, 16042 (1998).
- 20 W. Y. Ching, Journal of the American Ceramic Society **73**, 3135 (1990).
- 21 P. Hohenberg and W. Kohn, Physical Review **136**, B864 (1964).
- 22 W. Kohn and L. J. Sham, Physical Review **140**, A1133 (1965).
- 23 W. Y. Ching and P. Rulis, Physical Review B **73**, 045202 (2006).
- 24 W. Y. Ching, L. Ouyang, P. Rulis, and H. Yao, Physical Review B **78**, 014106 (2008).
- 25 W. Y. Ching and P. Rulis, Physical Review B **77**, 035125 (2008).
- 26 L. Liang, P. Rulis, B. Kahr, and W. Y. Ching, Physical Review B **80**, 235132 (2009).
- 27 S. Aryal, P. Rulis, and W. Y. Ching, American Mineralogist **93**, 114 (2008).
- 28 L. Liang, P. Rulis, and W. Y. Ching, Acta Biomaterialia **6**, 3763 (2010).
- 29 W. Y. Ching, S. Aryal, P. Rulis, and W. Schnick, Physical Review B **83**, 155109 (2011).
- 30 P. Rulis and W. Ching, Journal of Materials Science **46**, 4191 (2011).
- 31 P. Rulis, H. Yao, L. Ouyang, and W. Y. Ching, Physical Review B **76**, 245410 (2007).
- 32 W. Y. Ching, P. Rulis, L. Ouyang, and A. Misra, Applied Physics Letters **94**, 051907 (2009).
- 33 W. Y. Ching, P. Rulis, L. Ouyang, S. Aryal, and A. Misra, Physical Review B **81**, 214120 (2010).
- 34 L. Liang, P. Rulis, L. Ouyang, and W. Y. Ching, Physical Review B **83**, 024201 (2011).
- 35 R. S. Mulliken, The Journal of Chemical Physics **23**, 1841 (1955).
- 36 S. E. Lofland, J. D. Hettinger, K. Harrell, P. Finkel, S. Gupta, M. W. Barsoum, and G. Hug, Applied Physics Letters **84**, 508 (2004).
- 37 G. Hug, Physical Review B **74**, 184113 (2006).
- 38 J. H. Xu and A. J. Freeman, Physical Review B **41**, 12553 (1990).
- 39 J. H. Xu, T. Oguchi, and A. J. Freeman, Physical Review B **35**, 6940 (1987).
- 40 J. H. Xu and A. J. Freeman, Physical Review B **40**, 11927 (1989).

41 S. R. Nagel and J. Tauc, *Physical Review Letters* **35**, 380 (1975).
42 P. Ravindran and R. Asokamani, *Physical Review B* **50**, 668 (1994).
43 A. Ganguly, M. W. Barsoum, and J. Schuster, *Journal of the American Ceramic Society* **88**, 1290
(2005).
44 S. Amini, M. W. Barsoum, and T. El-Raghy, *Journal of the American Ceramic Society* **90**, 3953
(2007).
45 W. B. Tian, P. L. Wang, Y. M. Kan, G. J. Zhang, Y. X. Li, and D. S. Yan, *Materials Science and
Engineering: A* **443**, 229 (2007).
46 J. Etzkorn, M. Ade, and H. Hillebrecht, *Inorganic Chemistry* **46**, 1410 (2007).
47 G. Hug, M. Jaouen, and M. W. Barsoum, *Physical Review B* **71**, 024105 (2005).
48 W. Y. Ching and P. Rulis, *Electronic Structure Methods for Complex Materials: The orthogonalized
linear combination of atomic orbitals* (Oxford University Press, 2012).
49 C. Hu, L. He, J. Zhang, Y. Bao, J. Wang, M. Li, and Y. Zhou, *Journal of the European Ceramic
Society* **28**, 1679 (2008).
50 G. Yu, C. H. Lee, A. J. Heeger, and S. W. Cheong, *Physica C* **203**, 419 (1992).
51 T. H. Scabarozzi, et al., *Thin Solid Films* **517**, 2920 (2009).
52 O. Wilhelmsson, J. P. Palmquist, T. Nyberg, and U. Jansson, *Applied Physics Letters* **85**, 1066
(2004).
53 J. Emmerlich, H. Hogberg, S. Sasvari, P. O. A. Persson, L. Hultman, J. P. Palmquist, U. Jansson, J.
M. Molina-Aldareguia, and Z. Czigany, *Journal of Applied Physics* **96**, 4817 (2004).
54 T. H. Scabarozzi, et al., *Solid State Communications* **146**, 498 (2008).
55 T. Joelsson, A. Hoerling, J. Birch, and L. Hultman, *Applied Physics Letters* **86**, 111913 (2005).
56 E. H. Kisi, J. A. A. Crossley, S. Myhra, and M. W. Barsoum, *Journal of Physics and Chemistry of
Solids* **59**, 1437 (1998).
57 V. H. Nowotny, *Progress in Solid State Chemistry* **5**, 27 (1971).
58 Y. C. Zhou, H. Y. Dong, X. H. Wang, and S. Q. Chen, *Journal of Physics: Condensed Matter* **12**,
9617 (2000).
59 B. Manoun, R. P. Gulve, S. K. Saxena, S. Gupta, M. W. Barsoum, and C. S. Zha, *Physical Review B*
73, 024110 (2006).
60 A. L. Ivanovskii and N. I. Medvedeva, *Mendeleev Communications* **9**, 36 (1999).
61 J. C. Ho, H. H. Hamdeh, M. W. Barsoum, and T. El-Raghy, *Journal of Applied Physics* **86**, 3609
(1999).
62 D. Music, J. Emmerlich, and J. M. Schneider, *Journal of Physics: Condensed Matter* **19**, 136207
(2007).

Figure Captions:

Figure 1 Unit cell structures of Ta_2AlC , $\alpha-Ta_3AlC_2$, $\alpha-Ta_4AlC_3$, and Ta_5AlC_4 . (Color online)

Figure 2 Total and partial density of states for the 20 MAX-phase compounds.

Figure 3 $N(E_f)$ versus valence electron fillings. (a) In each colored series, A elements are from the same period of the periodic table, with different numbers of valence electrons. (b) 3 series: (3 1 2) phases with different A elements (olive green), (2 1 1) phases with different M (cyan), and X (magenta) elements. To show the $N(E_f)$ versus valence electron fillings of A, M and X elements respectively, Ti_2AlC appears 3 times, 1 in (a) and the other 2 in (b). (Color online)

Figure 4 Total (black) and partial (M-red, A-green, X-blue) density of states around Fermi-level for Ti_2InC , Ti_2SC , Cr_2AlC , Ti_2PC , Ti_2AsC , and Ta_5AlC_4 . (Color online)

Figure 5 Charge transfers in the 20 MAX-phase compounds. Hollow dark triangles denote the charge losses of M atoms. Solid blue dots (hollow blue circles) indicate the charge gains (losses) by A atoms. And the solid olive green triangles show the charge gains by X atoms. (Color online)

Figure 6 Different atomic sites in Ta_2AlC , $\alpha-Ta_3AlC_2$, $\alpha-Ta_4AlC_3$ and Ta_5AlC_4 . (Color online)

Figure 7 Optical conductivities of the 20 MAX-phase compounds. Blue curves show the planar component; Red curves show the axial component. (Color online)

Figures:

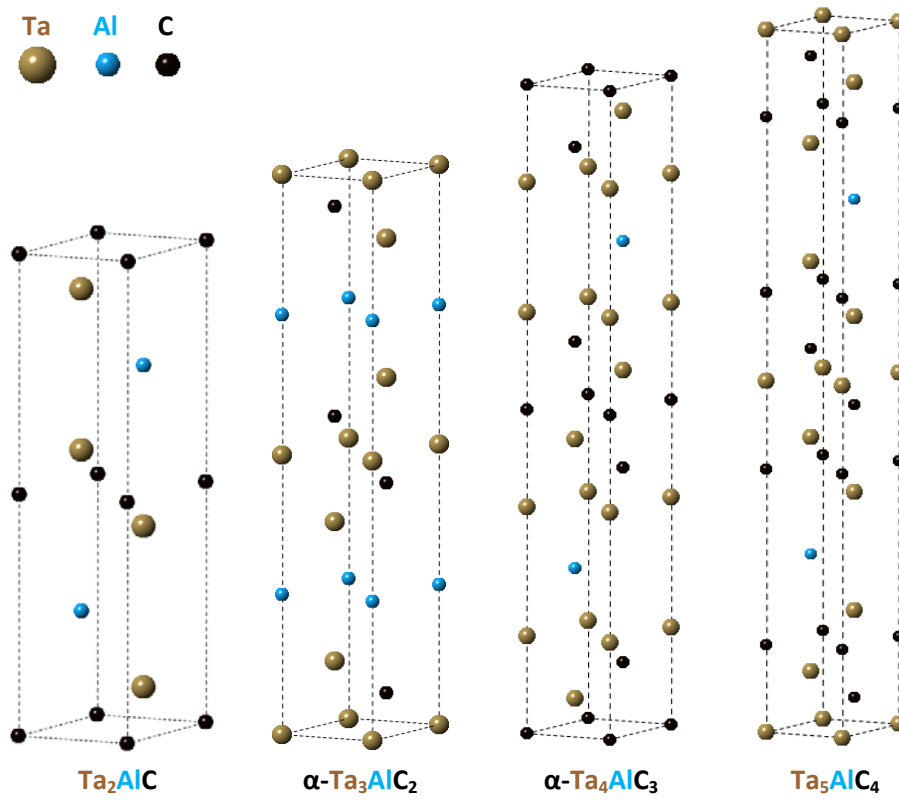


Figure 1

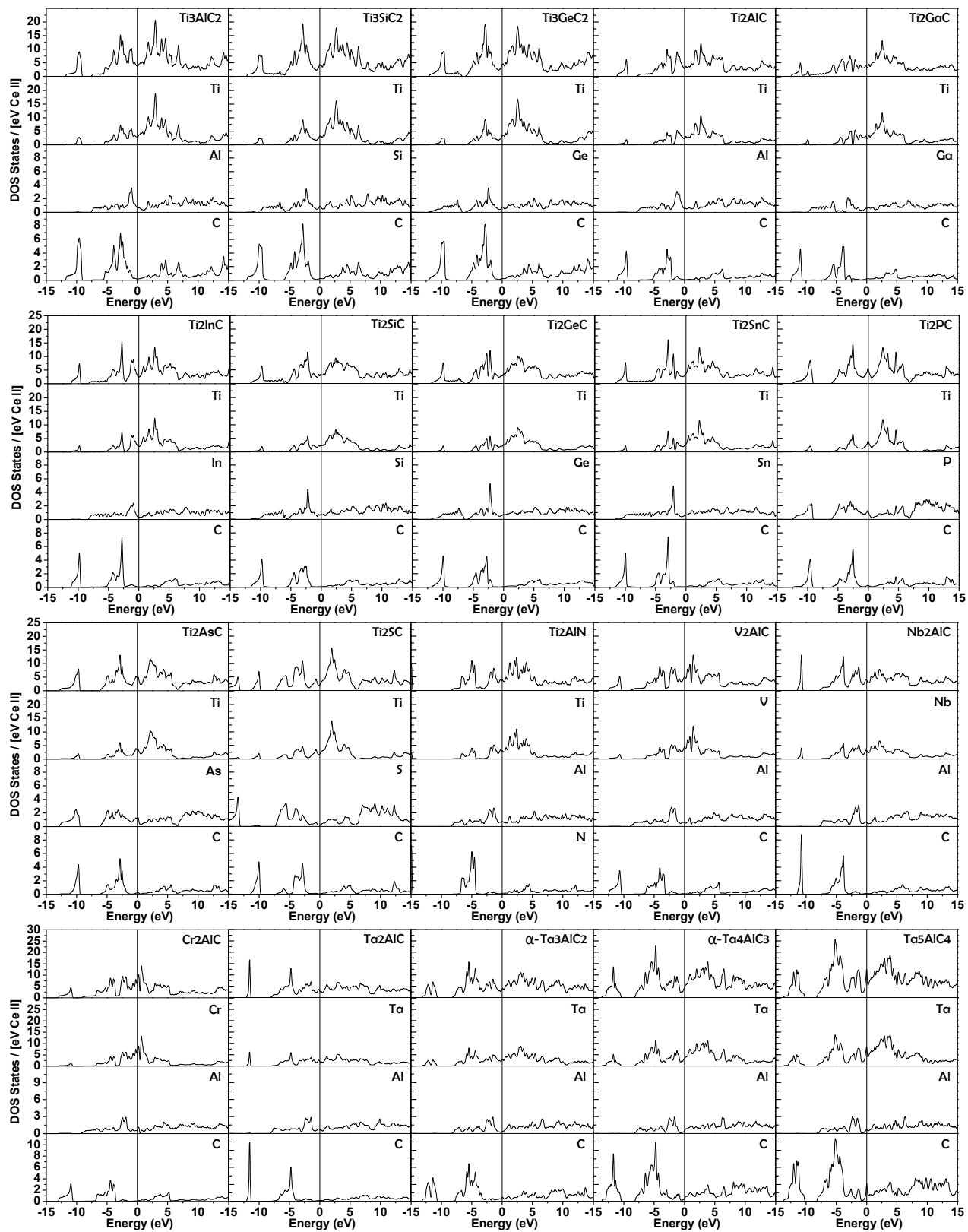


Figure 2

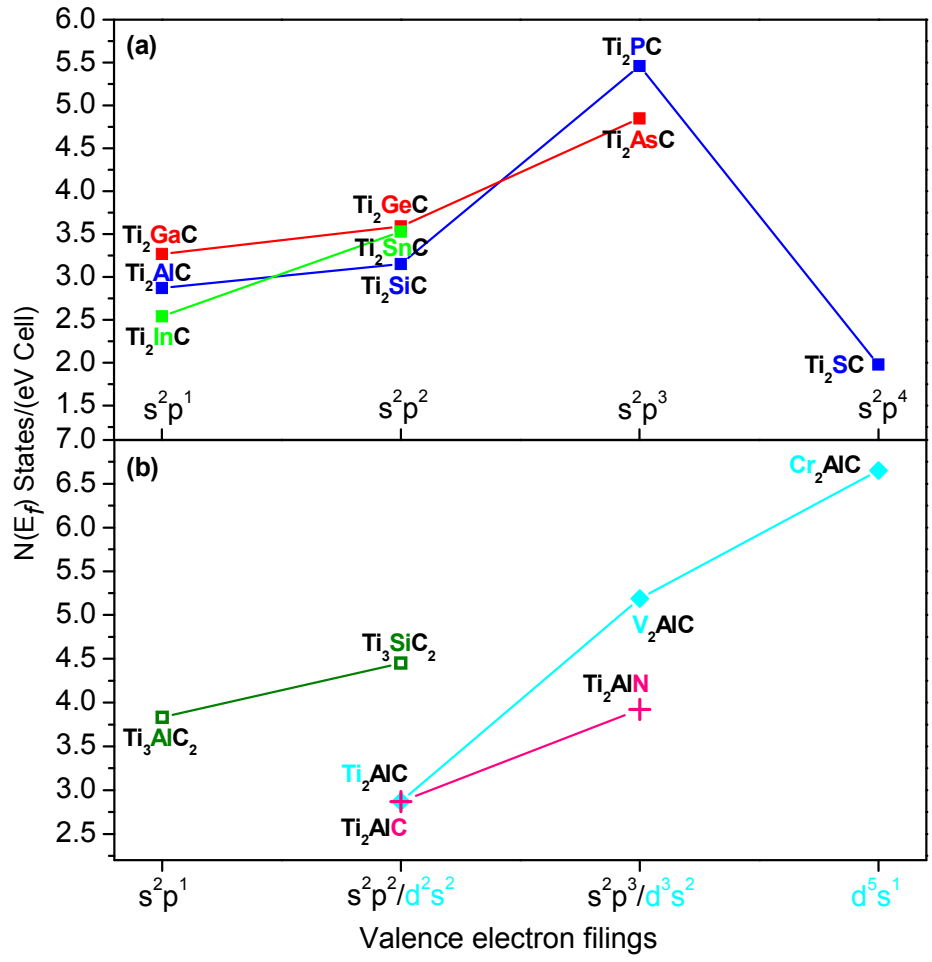


Figure 3

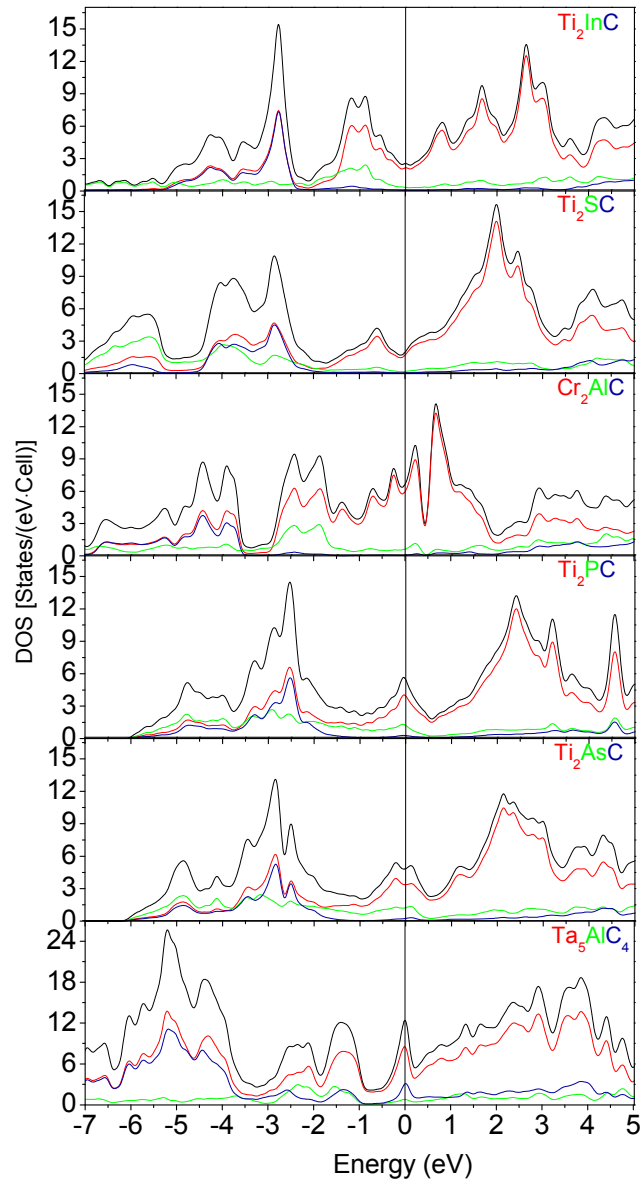


Figure 4

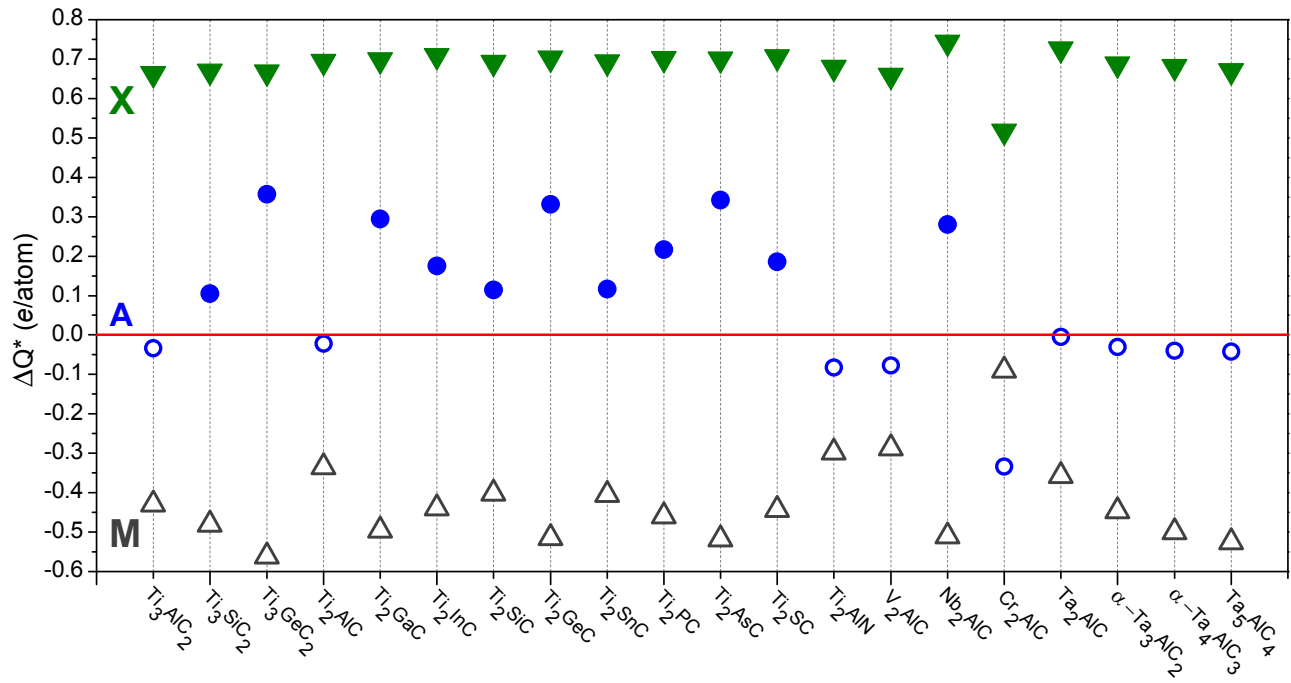


Figure 5

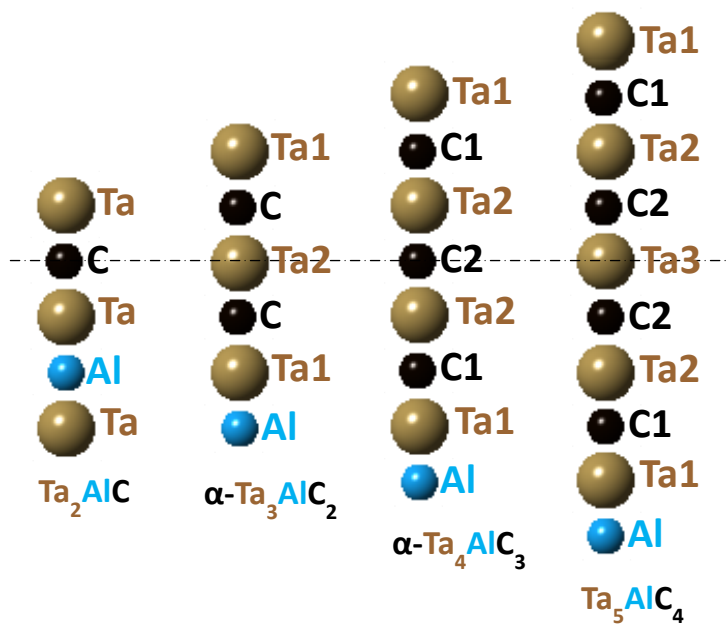


Figure 6

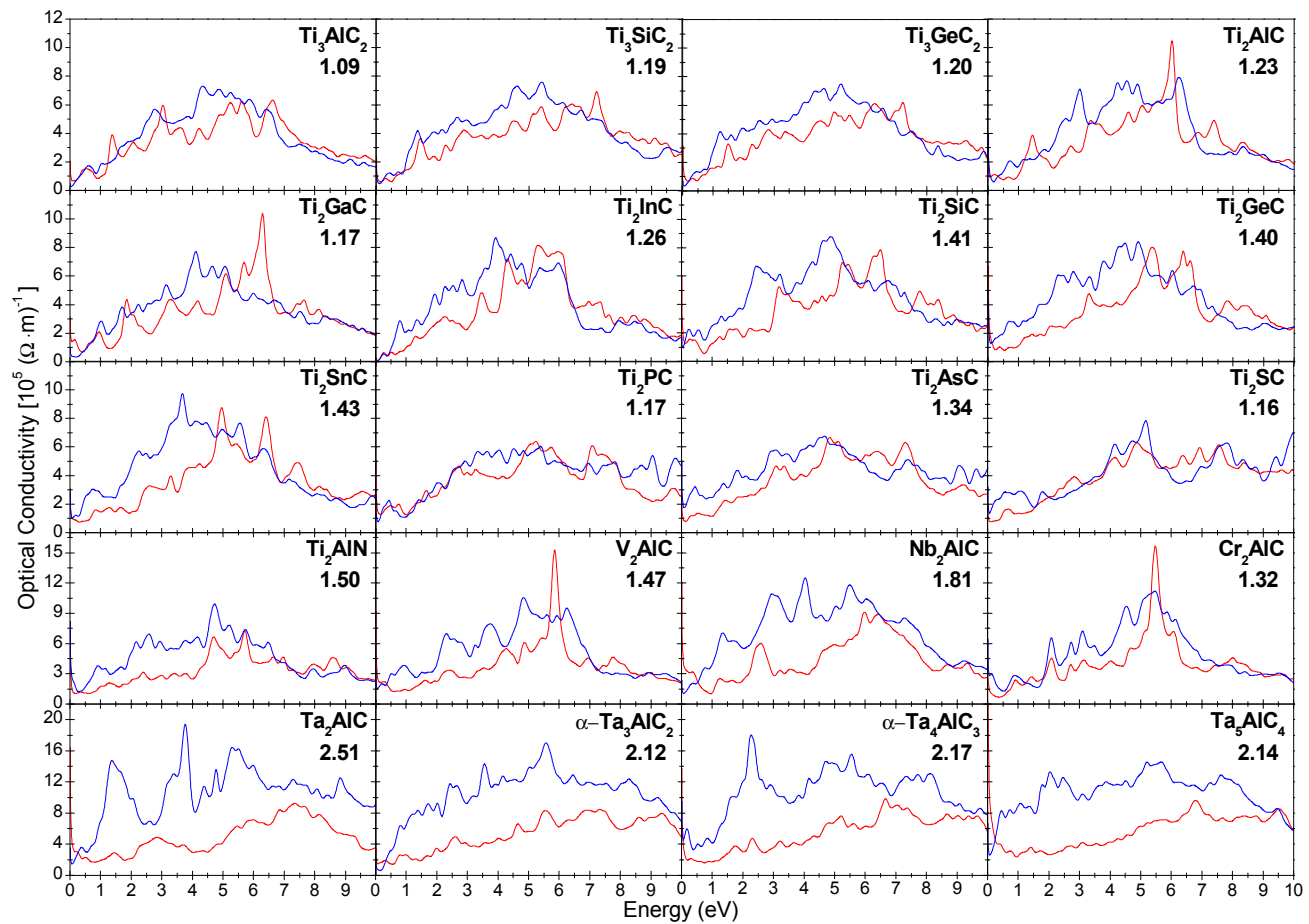


Figure 7